energies

MDPI

Article

Numerical and Experimental Investigations of CH_4/H_2 Mixtures: Ignition Delay Times, Laminar Burning Velocity and Extinction Limits

Simon Drost [1,*], Sven Eckart [2,*], Chunkan Yu [1], Robert Schießl [1], Hartmut Krause [2] and Ulrich Maas [1]

[1] Institute of Technical Thermodynamics, Karlsruhe Institute of Technology (KIT), 76131 Karlsruhe, Germany
[2] Institute of Thermal Engineering, Technische Universität Bergakademie Freiberg (TUBAF), 09599 Freiberg, Germany
* Correspondence: simon.drost@kit.edu (S.D.); sven.eckart@iwtt.tu-freiberg.de (S.E.)

Abstract: In this work, the influence of H_2 addition on the auto-ignition and combustion properties of CH_4 is investigated experimentally and numerically. Experimental ignition delay times (IDT) are compared with simulations and laminar burning velocities (LBVs), and extinction limits/extinction strain rates (ESRs) are compared with data from the literature. A wide variety of literature data are collected and reviewed, and experimental data points are extracted for IDT, LBV and ESR. The results are used for the validation of existing reaction mechanisms. The reaction mechanisms and models used are able to reproduce the influence of H_2 addition to CH_4 (e.g., shortening IDTs, increasing ESRs and increasing LBVs). IDTs are investigated in a range from 6 to 15 bar and temperatures from 929 to 1165 K with H_2 addition from 10 to 100 mol%. We show that LBV and ESR are predicted in a wide range by the numerical simulations. Moreover, the numerical simulations using detailed Aramco Mech 3.0 (581 species) are compared with the derived reduced reaction mechanism UCB Chen (49 species). The results show that the reduced chemistry obtained by considering only the IDT is also valid for LBV and ESR.

Keywords: methane; hydrogen; ignition delay times; rapid compression machine; laminar burning velocity; extinction limit

check for updates

Citation: Drost, S.; Eckart, S.; Yu, C.; Schießl, R.; Krause, H.; Maas, U. Numerical and Experimental Investigations of CH_4/H_2 Mixtures: Ignition Delay Times, Laminar Burning Velocity and Extinction Limits. *Energies* **2023**, *16*, 2621. https://doi.org/10.3390/en16062621

Academic Editor: Adonios Karpetis

Received: 15 December 2022
Revised: 25 February 2023
Accepted: 28 February 2023
Published: 10 March 2023

1. Introduction

Auto-ignition processes of methane (CH_4) and hydrogen (H_2) have been investigated for the pure substances. However, there is an increasing interest in mixtures of CH_4 and H_2. For example, there are investigations by several groups [1–3] on combustion in SI engines, using CH_4/H_2 mixtures investigating the peak temperature and NOx production. Petersen et al. [4] investigated lean CH_4/H_2 mixtures for gas turbine combustion, and Adolf et al. [5] and Melaina et al. [6], for example, investigated the addition of H_2 to the natural gas grid. In addition to these technical uses of CH_4/H_2 mixtures, there is also a safety aspect [7], for example, in nuclear power plants, as Rudy et al. [8] shows, or in pipelines/gas-processing sites as studied by Lowesmith et al. [9]. In addition, CH_4 (a main component of natural gas) and H_2 are very common fuels and are handled as fuels for greenhouse gas reduction [10,11].

A brief overview of studies investigating the ignition delay times (IDT) of CH_4/H_2 is summarized in Table 1 without claiming completeness. The studies are categorized by their setup (ST: shock tube and RCM: rapid compression machine) and sorted by year of publication. Regarding the fuel composition, the column named H_2 represents the mole fraction of H_2 in the CH_4/H_2 mixture (0 corresponds to pure CH_4, and 100 corresponds to pure H_2).

Table 1. Overview of the studies that investigated ignition delay times for CH_4/H_2 mixtures. Column H_2 represents the H_2 mole fraction in the fuel mixture of CH_4/H_2. RCM: rapid compression machine and ST: shock tube.

Setup	Author, Year	T / K	p / bar	H_2 in Fuel/ mol−%	Source
RCM	Lee, 1998	950–1050	6–40	100	[12]
RCM	Mittal, 2006	950–1100	15–50	100	[13]
RCM	Gersen, 2008	950–1060	15–70	0–100	[14]
RCM	Donohoe, 2014	930–1050	10, 30	60, 80	[15]
RCM	Hashemi, 2016	800–1250	15–80	0	[16]
RCM	Kéromnès, 2013	914–1014	8–70	100	[17]
ST	Bhaskaran, 1973	800–1400	2.5	100	[18]
ST	Slack, 1977	980–1176	2	100	[19]
ST	Wang, 2003	900–1350	3–17	100	[20]
ST	Huang, 2004	1000–1350	16–40	0	[21]
ST	Petersen, 2007	1132–1553	18–30	20, 40	[4]
ST	Pang, 2009	908–1118	3–4	100	[22]
ST	Zhang, 2012	1000–2000	5–20	0–100	[23]
ST	Kéromnès, 2013	925–2100	1–33	100	[17]
ST	Donohoe, 2014	1100–1700	1–30	30, 80	[15]
ST	Hu, 2016	850–1500	1–16	100	[24]

Hu et al. [24] measured IDT in an ST and compared the results to twelve reaction mechanisms. Based on [24], the H_2 IDT data is simulated in this work by the reaction mechanism from [25]. Focusing on the CH_4/H_2 mixtures from Table 1, Gersen et al. [14] investigated IDT in a pressure range between 15 and 70 bar and showed that the CH_4/C_3H_8 reaction mechanism of Petersen et al. [26] predicts the IDT for pure CH_4 and also for pure H_2 better than for their CH_4/H_2 mixtures. Donohoe et al. [15] measured IDT in an ST and a RCM, as well as flame speeds, of CH_4/H_2 mixtures and validated a former version of the AramcoMech (version 1.3) with these data.

As mentioned above, Petersen et al. [4] investigated the IDT of two CH_4/H_2 mixtures in gas turbines in comparison to other CH_4/alkanes mixtures. They found a significantly reduced IDT by adding H_2. This effect is further investigated in this current work. Zhang et al. [23] studied lean ($\phi = 0.5$) CH_4/H_2 mixtures in a shock tube. Under their conditions, they found a mixture of 40/60 CH_4/H_2 (molar) was almost independent of pressure. Under the aspect of new technical applications, it makes sense to improve the data on the ignition and combustion properties of CH_4/H_2 mixtures through dedicated experiments.

For the laminar burning velocity (LBV), numerous experiments have been conducted under different conditions over the last fifteen years. The addition of H_2 to CH_4 regarding the LBV has been investigated both numerically, e.g., [27,28], and experimentally. An overview of these experiments is given in [29] and in Table 2. The experimental data (see Table 2) were generated with different setups that are described in more detail in [30]. It can be seen that all methods except SEF were applied only under atmospheric conditions. The measurements that are known to us terminate at a pressure of 7.5 bar [31] and a temperature of 650 K [32]. In the high-temperature region, however, only hydrogen admixtures up to 50 mol−% are considered.

For higher pressures, values up to 100 mol−% of H_2 in fuel are available. As expected, the trend indicates that the LBV increases over the entire mixing range when temperatures rise. A clear increase in LBV can also be observed for increasing hydrogen fractions with an increase in admixture up to about 50% in a linear fashion and exponentially beyond this point. For the pressure dependence, inconsistencies are found in the literature [30]; this is particularly applicable for higher (80% H_2) hydrogen admixtures. For low admixtures, the LBV decreases with increasing pressure.

Table 2. Overview of the studies that investigated the laminar burning velocity for CH_4/H_2 mixtures. Column H_2 represents the H_2 mole fraction in the fuel mixture of CH_4/H_2. BB: Bunsen burner; SB: slotburner; CEV: Cardiff explosion vessel; CF: counterflow; CV: combustion vessel; SEF: spherical expanding flame; HF: heat flux burner; and EHC: external heated converging channel.

Setup	Author, Year	T / K	p / bar	H_2 / mol−%	Source
BB	Braun-Unkhoff, 2009	373	1	50	[33]
SB	Boushaki, 2012	300	1	0–30	[34]
SB	Göckeler, 2013	440	1	0–50	[35]
SB	Lhuillier, 2017	393–473	1	0–80	[36]
CEV	Ilbas, 2006	298	1	0–100	[37]
CF	Park, 2011	298	1	95	[38]
CF	Li, 2017	283	1	0–50	[39]
CV	Cammarota, 2009	298	1	10	[40]
SEF	Halter, 2005	298	3,5	0–20	[41]
SEF	Halter, 2007	298	1	0–20	[42]
SEF	Shy, 2008	298	1	0–30	[43]
SEF	Miao, 2009	298	1	20	[44]
SEF	Tahtouh, 2009	300	1	0–30	[45]
SEF	Hu, 2009a	303	1	0–100	[31]
SEF	Hu, 2009b	303–443	1–7.5	0–80	[46]
SEF	Hu, 2009c	303–443	1–7.5	0–80	[47]
SEF	Fairweather, 2009	360	1	0–50	[48]
SEF	Salzano, 2012	293	1–6	0–100	[49]
SEF	Okafor, 2014	350	1	0–100	[50]
SEF	Donohoe, 2014	300	1	50	[15]
SEF	Troshin, 2014	293–573	1–10	0–20	[51]
SEF	Reyes, 2017	300	1	0–100	[52]
SEF	Khan, 2019	300	1	20	[53]
SEF	Morovatiyan, 2019	298–440	1	0–20	[54]
SEF	Cai, 2020	298	1	20–80	[55]
SEF	Nguyen, 2022	298	1	0–50	[56]
HF	Coppens, 2007	298	1	0–35	[57]
HF	Hermanns, 2007	298–433	1	0–40	[58]
HF	Dirrenberger, 2011	298	1	0–67	[59]
HF	Nilsson, 2017	298	1	0–50	[60]
HF	Jithin, 2020	300	1	0–40	[61]
HF	Wang, 2018	298	1	0–40	[62]
HF/SEF	Eckart, 2022	298–373	1–5	0–50	[63]
EHC	Berwal, 2022	300–650	1	0–50	[64]

In comparison to LBV, the extinction strain rate has only been considered in very few experimental studies. An overview of these experiments is given in in Table 3. In the premixed flames [7,65], this may primarily relate to the very high outflow velocities that occur. In the non-premixed case [66,67], there are also only two known studies, for which the increased complexity in the precise dosing of very small amounts of hydrogen (mass-related) could be the determining factor. To the best of our knowledge, neither premixed nor non-premixed studies are known that have investigated a content of above 40 mol−% H_2 admixture in CH_4. This represents a clear gap in the literature.

Table 3. Overview of the studies that investigated extinction strain rates for CH_4/H_2 mixtures. Column H_2 represents the H_2 mole fraction in the fuel mixture of CH_4/H_2. CF: counterflow.

Setup	Author, Year	T / K	p / bar	H_2 / mol−%	Mode	Source
CF	Jackson, 2003	573	1	0–20	premixed	[65]
CF	Yang, 2022	298	1	0–40	premixed	[7]
CF	Niemann, 2013	298	1	0–18	non-premixed	[66]
CF	Eckart, 2022	298	1	0–100	non-premixed	[67]

As can be seen from Tables 1–3, there are several experimental data available for CH_4 and H_2 mixtures. Recently, Eckart et al. [67] covered the range 0–100% of H_2 mixed to CH_4 for ESRs; however, the setup was limited to low temperatures. In Eckart et al. [63], they used two setups for the LBV measurements with setup limits (5 bar and 373 K). In a small range of conditions, Troshin et al. [51] measured LBVs up to 10 bar (293–573 K), and Berwal et al. measured up to 650 K (1 bar) [64]. Considering the IDT, data for CH_4/H_2 mixtures are still missing in wide areas. Gersen et al. [14] already provided preliminary work but only higher than 15 bar and only for a limited temperature range. This range will be therefore widened by the recent work.

In this work, we mainly investigated four stoichiometric CH_4/H_2 mixtures (0/100, 50/50, 80/20 and 90/10 CH_4/H_2, molar) in regard to their auto-ignition properties. For this purpose, IDTs were measured experimentally in an RCM and compared with simulations. All experimental results were compared with a detailed (AramcoMech 3.0 [68]) and an associated reduced (UCB Chen [69]) reaction mechanism.

As stated earlier, IDT is only one of the relevant validation targets for detailed and reduced reaction mechanisms. Therefore, after a detailed sensitivity analysis for the IDTs, the influence of the reduction of the mechanism on the other validation parameters of the laminar burning velocity and the extinction strain rate were again examined.

2. Methodology

2.1. Rapid Compression Machine: Experiment

The experiments were performed in a rapid compression machine (RCM), which is explained in detail in [70–72]; a brief overview of that RCM is given here. Figure 1 depicts the experimental setup of the RCM and the experiment.

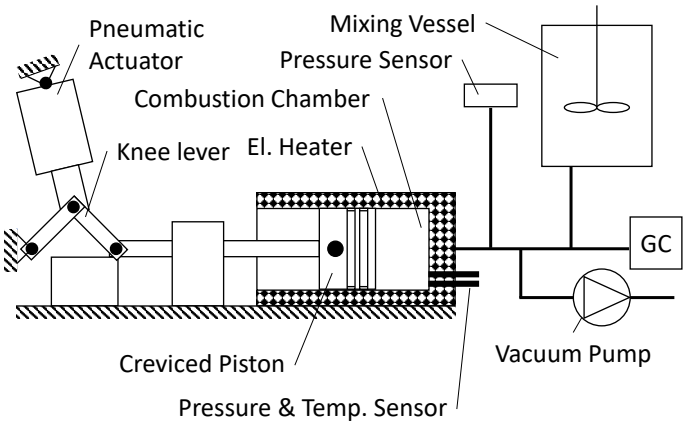

Figure 1. Schematic of the main components of the RCM experiment. Adapted from [70].

The RCM is a piston-cylinder device with a compression time between 20 and 40 ms. The compression takes place under well-defined, reproducible initial and boundary conditions with regard to the pressure, temperature and gas composition. At top dead center (TDC), the piston is fixed with a mechanical lock, consisting of a knee-lever construction, whereby an isochoric state of the combustion chamber is forced. The initial pressure p_0 in the combustion chamber is measured with an absolute pressure sensor (MKS Baratron 121A, [73]) with a relative accuracy of 0.5%. The initial temperature T_0 is measured with a type-K thermocouple (accuracy of 2.2 K) [74] and can be adjusted by heating between 320 and 470 K. The gas mixtures to be investigated are prepared in a mixing vessel (about 10 L).

The volume and the pressure in the mixing vessel are higher than the initial pressure and the initial volume in the combustion chamber. This minimizes the measurement inaccuracy in the production of the initial gas. The combustion chamber of the RCM is filled with gas from the mixing vessel. After filling, an RCM experiment is performed. The temporal pressure trace in the combustion chamber is measured with a quartz pressure sensor (Kistler 6061 B [75])

with a linearity of ≤0.5%. In the investigated temperature range, the mentioned uncertainties result in temperature uncertainties of approximately ±7 K. The time-resolved piston position is detected with a linear position sensor/potentiometer (Burster type 8712 [76]). The linear position sensor has a linearity of 0.1%.

Figure 2 (left) shows the pressure trace as measured in an experiment.

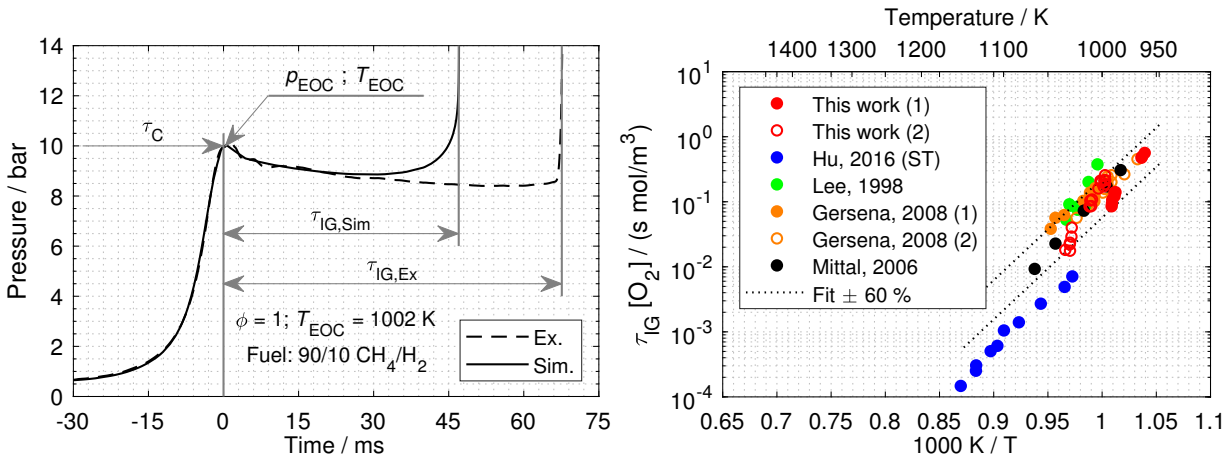

Figure 2. (**Left**): Pressure trace of an RCM experiment with its corresponding simulation (same initial conditions, p_0 = 0.6 bar, T_0 = 411 K). (**Right**): Ignition delay times of H_2 at stoichiometric conditions scaled by the O_2 concentration compared with data from the literature. Data from: Gersen, 2008 (1&2) [14], Hu, 2016 [24], Lee, 1998 [12] and Mittal, 2006 [13].

In this study, an RCM experiment is characterized by the pressure and temperature after the end of compression (index EOC, Figure 2 (left)). At TDC and isochoric conditions, however, heat losses occur, and this results in a temperature and pressure drop after compression. Ignition is detected by a rapid increase in pressure. The time measured between the end of compression and ignition is the ignition delay time (IDT, τ_{IG}).

In measuring the IDT in an RCM, effects (such as heat losses, dilution and pressure) can vary from facility/experiment to facility/experiment and, thus, influence the IDT. Therefore, for validation purposes, the H_2 IDT data from this study is compared to the results of other publications (results for stoichiometric mixtures at pressure $p_C > 10$ bar). Experiments listed in Table 1 matching these criteria are listed with additional information in Table 4.

Table 4. Overview of IDT as shown in Figure 2 for pure H_2 and stoichiometric conditions.

Setup	Inert/O_2	p / bar	Source
RCM	3.76	≈ 10	This work (1)
RCM	9	≈ 10	This work (2)
RCM	5	16–21	Gersen (1) [14]
RCM	5	20–50	Gersen (2) [14]
ST	30.8	10	Hu [24]
RCM	5	≈ 10	Lee [12]
RCM	13	15	Mittal [13]

To minimize the effects of different dilutions (Inert/O_2 ratio) and different compression pressures (p_{EOC}) of the compared studies, we scaled the IDT by the O_2 concentration ([O_2]) as proposed by [12]:

$$\tau_{IG}[\mathrm{O_2}] = \tau_{IG}\frac{p_{EOC}X_{\mathrm{O_2}}}{RT_{EOC}} \quad (1)$$

with τ_{IG} as the IDT of a dedicated experiment, $X_{\mathrm{O_2}}$ as the corresponding mole fraction, R as the gas constant and T_{EOC} as the temperature at the end of compression. For these

calculations, the ideal gas law was assumed. The comparison of the studies by the scaled IDT is shown in Figure 2 (right), whereby different colors denote different RCM facilities with different heat losses (except [24] (blue bullets) with a shock tube). H_2 is one of the most frequently measured fuels in RCMs and STs apart from CH_4; however, our CH_4 data were already published in [69], and we, therefore, chose H_2 here. The IDT results of the mentioned studies and our work show good agreement. Based on the depicted IDTs from RCM experiments, an Arrhenius-like fitting curve was calculated,

$$\tau_{IG}[\mathrm{O_2}] = A^* \exp(E^*/T), \tag{2}$$

with $A^* = 3.3 \times 10^{-17}\,\mathrm{smol/m^3}$, $E^* = 3.6 \times 10^4\,\mathrm{K}$ and T as the temperature. The data of the different RCM studies are in a band of ±60% for this fit. The shock tube data from Hu et al. [24] vary from this band—caused by the different setup and the very high dilution [77].

2.2. Rapid Compression Machine: Model

Simulations were performed using the in-house code HOMREA [78]. IDTs were simulated using the adiabatic core assumption [79,80]. We assumed that, despite the heat losses of the hot gas to the combustion chamber walls, an adiabatic gas (adiabatic core) remains in the middle of the combustion chamber. This adiabatic core delivers work to the surrounding gas layer, which causes a change of the internal energy and, thus, in the temperature of the core gas. The effective volume $v(\tau)$ of the adiabatic core is calculated from a measured pressure curve as follows,

$$\int_{v_0}^{v(t)} \frac{c_p(T)}{c_v(T)} \frac{1}{v} \mathrm{d}v = \ln\left(\frac{p_0}{p(t)}\right). \tag{3}$$

Here, $c_p(T)$ and $c_v(T)$ are the temperature-dependent specific heat capacities of the gas mixture, v_0 is the initial volume, p_0 is the initial pressure, and $p(t)$ is the experimentally measured pressure of a non-reacting gas mixture. In the experiment with the non-reacting gas mixture, O_2 was substituted with N_2, which resulted in a similar heat capacity and thermal conductivity to the corresponding oxygen-containing mixture; however, there was no chemical reaction at the conditions of interest [81,82].

Due to the non-reacting gas mixture, only the influence of heat losses, which are not influenced by the chemistry, was measured. The adiabatic core assumption is sufficient for ignition delay times less than 100 ms [83]. Figure 2 (left) shows the pressure trace measured in the experiment and the pressure trace simulated with the adiabatic core model under nominally the same initial conditions. The pressure trace—in particular, the pressure drop after compression by heat loss and the pressure increase by the combustion after ignition—is reproduced by the simulation.

2.3. Heat-Flux Burner: Model

For comparison with the experimental LBV data, freely propagating one-dimensional flames were investigated numerically with the laminar premixed flamespeed code of Chemkin-Pro 2020 R2 [84]. The laminar burning velocity is a fundamental quantity present in a flat unstretched flame; it can be adequately calculated with a 1D prediction [30]. The LBV was calculated using multicomponent transport coefficients with a thermal diffusion option (Soret effect). The number of grid points was set to 1300 with respect to the gradient (GRAD = 0.04) and curvature (CURV = 0.08) adaptive mesh parameters. Further details are explained in the work of Eckart et al. [85].

2.4. Extinction Limits: Model

The in-house code INSFLA [78,86] was used to calculate the extinction strain rate (ESR) for the counterflow flame. In our model, the detailed transport models, including differential diffusion of different species and the thermal diffusion (the Soret effect) were

included [87]. The optical thin model (OTM) for thermal radiation was also considered as documented in [88]. The detailed description of the ESR determination is consistent with that in our previous paper [89]. Note that the extinction limits were determined by using one-dimensional simulations. It was shown in our previous paper [89] that this is sufficient for the accuracy of the extinction limits. Nevertheless, two-dimensional simulations would further improve the accuracy.

2.5. Reaction Mechanisms

In this work, two different reaction mechanisms are used. First, the detailed reaction mechanism ArmacoMech 3.0 [68] was applied. This reaction mechanism consists of 581 species and 3037 reactions. The AramcoMech 3.0 was built by a H_2/CO sub-reaction mechanism [17] and a C1−C2 reaction mechanism [90]. The (sub)-reaction mechanisms have already been validated for a large database, such as IDTs, LBVs and species formation in flow reactors [17,68,90]. Due to the size of the AramcoMech 3.0, it is less suitable for very complex models, such as DNS simulations, which are usually performed with smaller reaction mechanisms [91,92]. Therefore, the AramcoMech 3.0 was reduced in a previous work to better reflect the C1−C3 chemistry (UCB Chen [69]). The UCB Chen consists of 49 species and 332 reactions [72] and can also be used as a base reaction mechanism (C1−C3) for other reduced reaction mechanisms, e.g., it was extended for ethanol combustion [72].

3. Results

3.1. Influence of CH_4/H_2 Ratio

Figure 3 (left) depicts the IDT results from experiments and 0D simulations with an effective volume profile. Four different fuel blends at a pressure of 10 bar are shown. The AramcoMech 3.0 reaction mechanism shows good agreement for the 90/10 CH_4/H_2 mixture and for pure H_2. The IDT results of the experiment and simulation of the other two mixtures diverge with decreasing temperature. The IDTs of mixtures with an intermediate ratio of CH_4/H_2 were predicted as too short by the AramcoMech 3.0 [68]. A similar effect was observed by Gersen et al. [14] for the reaction mechanism of Petersen et al. [26].

Panigrahy et al. [93] found several reactions that are important for CH_4/H_2 mixtures but less important for pure CH_4 or pure H_2. One reaction is $CH_4 + H\cdot \rightleftharpoons CH_3\cdot + H_2$ [93]. The parameters of this reaction are different in the Aramco Mech 3.0 [68] in comparison to the NUI Galway Mech studied in the work of Panigrahy et al. [93]. However, the trend was still captured well for all mixtures. The trend of the experimental data suggests that the IDTs merge at low temperatures. This trend was also predicted by the numerical simulations.

At lower temperatures, the difference in IDT for CH_4 and H_2 decreased. When the temperature decreased further, the H_2 ignition became slower than for CH_4 as shown by Panigrahy et al. [93]. This is explained by the higher reactivity of $CH_3\cdot$ in comparison to H atoms at low temperatures [93]. Figure 3 (left) demonstrates, on the one hand, the ignition-enhancing effect of H_2 in the fuel and, on the other hand, the increase of the apparent activation energy with increasing H_2 fraction. To analyze the ignition-enhancing effect of H_2 in a CH_4/H_2 mixture in more detail, Figure 3 (right) compares the IDTs of different simulations with varying H_2 mole fractions in fuel (black line). The simulations were each performed in an adiabatic, isochoric and homogeneous reactor with the same initial pressure and the same initial temperature. The H_2 content in fuel α mentioned in Figure 3 (right) is

$$\alpha = X_{H_2}/(X_{H_2} + X_{CH_4}) \tag{4}$$

with X_i as mole fractions. A stoichiometric mixture with a H_2 content of α leads to an oxygen ratio β, defined as

$$\beta = \nu_{H_2}\alpha + \nu_{CH_4}(1-\alpha) = 0.5\alpha + 2(1-\alpha) = 2 - 1.5\alpha \tag{5}$$

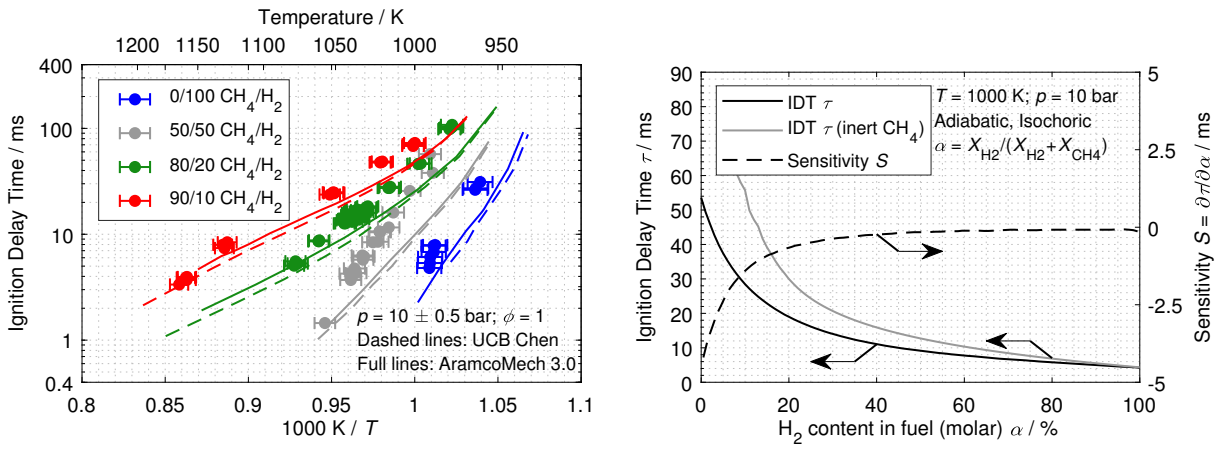

Figure 3. (**Left**): IDT experiments and simulations of different fuels at a constant pressure. Simulations were performed with the AramcoMech 3.0 [68] and UCB Chen [69] reaction mechanism. (**Right**): Sensitivity analysis of stoichiometric mixtures with varying CH_4/H_2 ratios in fuel. Simulations were performed with AramcoMech 3.0 [68].

with the stoichiometric coefficients ν_i and the assumption of a complete reaction to H_2O and CO_2. The Ar dilution is derived from air with a molar Ar/O_2 ratio of 3.76, resulting in a gas mixture with the following molar shares:

$$(1-\alpha)\ /\ \alpha\ /\ \beta\ /\ 3.76\beta \quad CH_4/H_2/O_2/Ar\ \text{(molar)}. \tag{6}$$

For pure CH_4 ($\alpha = 0$), the gas composition $CH_4/H_2/O_2/Ar$ is 1/0/2/7.52 (molar), and for a pure H_2 mixture ($\alpha = 1$), the gas composition is 0/1/0.5/1.88 (molar).

The simulations were performed with the AramcoMech 3.0 reaction mechanism [68], and they highlight the ignition-accelerating effect of H_2. The ignition-accelerating effect can be quantified by the sensitivity S of the IDT with respect to the change in the H_2 content α

$$S = \frac{\partial \tau}{\partial \alpha} \approx \frac{\tau(\alpha + 0.01) - \tau(\alpha)}{0.01}, \tag{7}$$

$\tau(\alpha)$ is the calculated IDT shown in Figure 3 (right) as a black line. The corresponding sensitivity according to Equation (7) is shown in Figure 3 (right) as a black dashed line. Low values of the H_2 content α (low H_2 mole fractions) were the most sensitive to increasing α, meaning that small additions of H_2 had the highest impact on reducing IDT at constant pressure/temperature. The more H_2 mixed into the fuel, the less sensitive the system becomes for H_2 addition according to the IDT. Note that, if CH_4 is treated as an inert species and everything else is kept constant, the reactants (H_2/O_2) no longer form a stoichiometric mixture but lean mixtures instead and, thus, ignite later than their stoichiometric counterparts [24].

Furthermore, the dilution of inert/O_2 increases, which generally leads to longer IDT—all other conditions being unchanged. CH_4 as an intert species adds a high heat capacity to the system without any ignition-supporting effect and, therefore, slows down the temperature rise during self-ignition.

Figure 4 shows the relative sensitivities of the OH radical (concentration). Full lines refer to positive sensitivities, and dashed lines refer to negative sensitivities. All sensitivities were calculated for an adiabatic and isochoric system for the time right before the gas mixture ignites ($0.9\tau_{IG}$). The initial conditions were $p = 10$ bar and $T = 1000$ K with a variable H_2 content α (CH_4/H_2 ratio, Equation (4) and a constant Ar/O_2 = 3.76 (molar) ratio.

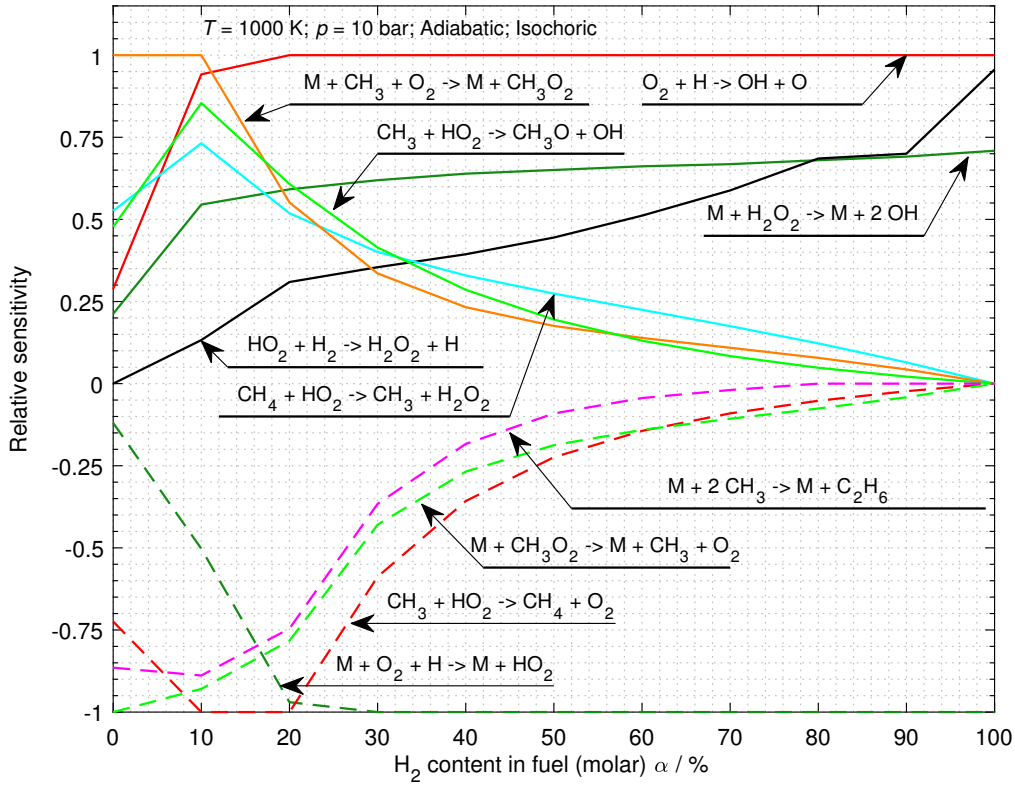

Figure 4. Sensitivity analysis of stoichiometric mixtures with varying CH_4/H_2 ratio α. Simulations were performed with AramcoMech 3.0 [68]. Full lines: positive sensitivities and dashed lines: negative sensitivities.

For pure CH_4 mixtures ($\alpha = 0$), the most sensitive reaction was

$$CH_3 + O_2 + M \rightleftharpoons CH_3O_2 + M.$$

For a high CH_4 mole fraction in the fuel, the following reaction producing methyl radicals ($CH_3\cdot$) was sensitive

$$CH_4 + HO_2 \rightleftharpoons CH_3 + H_2O_2.$$

On the other hand, with an increasing H_2 fraction, reaction

$$O_2 + H \rightleftharpoons O + OH$$

became the most sensitive, followed by two other hydrogen reactions. With respect to negative sensitivities, the formation of hydroperoxyl (HO_2) was the most sensitive reaction for compositions $\alpha > 21\%$

$$H + O_2 + M \rightleftharpoons HO_2 + M$$

However, this reaction loses sensitivity with an increasing CH_4 mole fraction (left side). Then, the consumption of $CH_3\cdot$ and $CH_3O_2\cdot$ radicals become important. A notable fact is that even an α as small as 5% led to high sensitivity with respect to the reaction $O_2 + H \longrightarrow OH + O$. This sensitive reaction also explains the high sensitivity of the IDT according the H_2 mole fraction in Figure 3.

3.2. Pressure Influence

Figure 5 (left) depicts the IDT of pure H_2 (full symbols) in comparison to the 80/20 CH_4/H_2 fuel mixture (open symbols) at pressures of 10 and 15 bar. All data points from

the simulations show shorter or the same IDT as the experiments. In the H_2 case, the experiments are compared to two reaction mechanisms, first the AramcoMech 3.0 reaction mechanism and a H_2 reaction mechanism [25]. Both reaction mechanisms reproduced the trend well and also calculated comparable values for the ignition delay time.

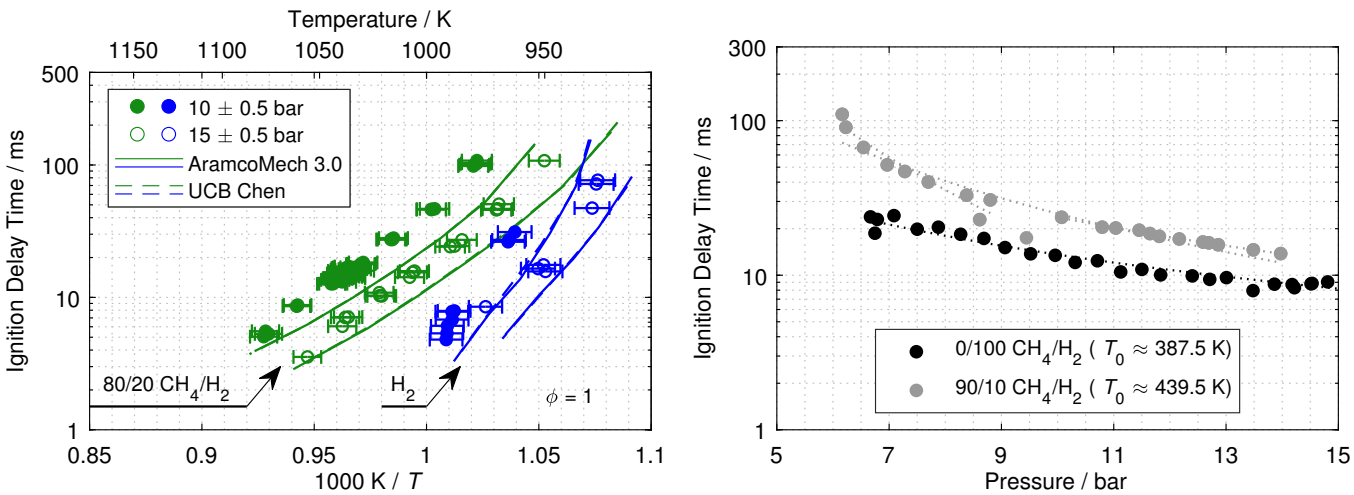

Figure 5. (**Left**): Comparison of a stoichiometric H_2 mixture (bullets) vs. stoichiometric 80/20 CH_4/H_2 mixture (open circles) at pressures of 10 ± 0.5 bar and 15 ± 0.5 bar. Simulations: AramcoMech 3.0 [68] (full lines) and UCB Chen [69] (dashed lines). (**Right**): IDT experiments of two fuels with a constant initial temperature and varying pressure. Lines are drawn to guide the eye.

When comparing the 80/20 CH_4/H_2 mixture versus pure H_2, both fuels show a linear decrease in the ignition delay time as a function of the temperature increase. Increasing the pressure results in a decrease in the ignition delay time in the investigated pressure/temperature regimes. In comparison, the 80/20 CH_4/H_2 mixture ignites slower than pure H_2 at equivalent pressure and temperature. The temperature sensitivity decreases for the CH_4/H_2 mixture compared to pure H_2 (the slope in the Arrhenius diagram).

Figure 5 (right) compares the ignition delay times of a fuel mixture of 90/10 CH_4/H_2 and pure H_2 as a function of pressure. The compression temperatures for both gas mixtures are in a narrow temperature range since the initial temperature is held constant. The compression temperature of the CH_4/H_2 mixture is T_C = 1040–1070 K, and the compression temperatures for the pure H_2 experiments are between T_C = 970 and 1000 K. Increasing the compression pressure from $p_C = 6$ to 15 bar, the IDT drops for both fuels. Here, the CH_4/H_2 mixture shows a stronger pressure dependence for the IDT when compared with H_2.

3.3. Laminar Burning Velocity

In addition to the new IDT measurements, the numerical models were also compared against other experiments from the literature. Therefore, LBV and ESR experiments, as listed in Table 2, were selected. In Figure 6, the laminar burning velocities of CH_4/H_2 mixtures are shown.

The mixtures are 100/0, 80/20, 60/40, 40/60 and 20/80 CH_4/H_2 (molar). In addition, the LBVs were calculated for temperatures of the gases at 298, 373, 473 and 573 K. Here, the two numerical models, AramcoMech 3.0 [68] (dashed line) and UCB Chen [69] (solid line) are compared. Furthermore, the experimental data from Table 2 are presented. The data are not assigned to the individual measurement series but only serve to determine the range in which a scattering of experimental data is present in the literature.

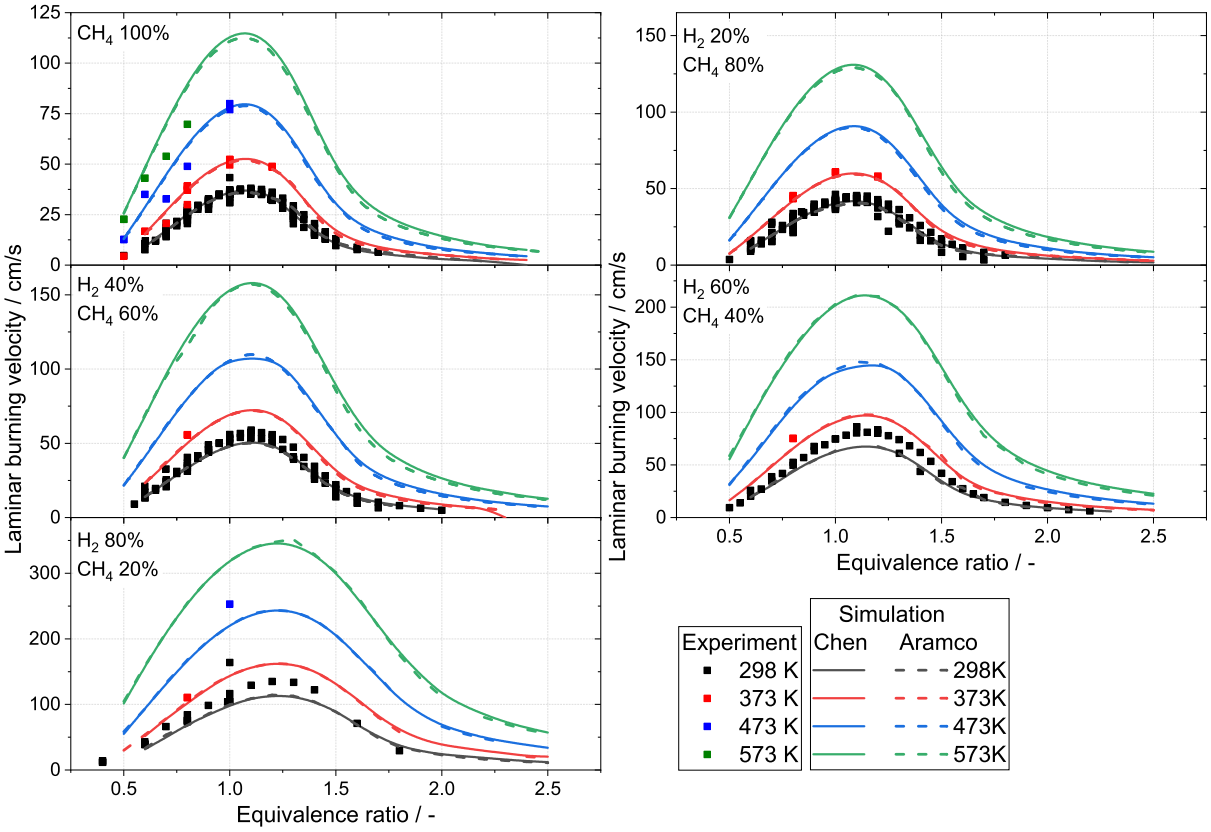

Figure 6. Comparison of the laminar burning velocity of a methane–hydrogen mixture ($p = 1$ bar) for different temperatures (298 , 373 , 473 and 573 K) to the experimental literature data from Table 2.

When evaluating the data, it is clear that the LBV increases with higher temperatures in all equivalence ratio ranges as expected. For temperatures above 373 K, only very few data sets are available [29,63], which clearly complicates the validation of the detailed reaction mechanisms. For CH_4, experimental data are available for all four temperature ranges—at least in the lean range. However, above 373 K, the few data for CH_4 are clearly overestimated by the models. For the range below 373 K, a good agreement between the reaction mechanisms and the experimental data can be found for all stages of CH_4/H_2 mixtures.

However, the agreement decreases for 60–80 mol−% H_2, and a slight underestimation of certain data sets is observed. Comparing AramcoMech 3.0 with the UCB Chen reaction mechanism, no significant differences were found. This can be assumed to be because the UCB Chen reaction mechanism was developed by reducing AramcoMech 3.0. During development, laminar burning velocity values were also a target to be reproduced by the reduced mechanism.

For higher temperatures (above 373 K) there are currently not enough data available to make a comprehensive comparison. However, it is already evident from the CH_4 data that the two mechanisms significantly overestimate the values in the lean range. Simulations of the stoichiometric 80 mol−% H_2 mixtures and 473 K show an underestimation of the measurement results. As already mentioned, there are currently only a few studies available that have measured both high temperatures and high H_2 contents (see Table 2).

From these comparisons follow some suggestions for future work. Since a validation of the reaction mechanisms for LBV above 373 K is hardly possible, experiments should be performed in these temperature ranges for which some existing spherical chambers as well as diverging channel setups are suitable. Furthermore, this is particularly the case for H_2 admixtures above 60%, where significantly less data are available. Only then could the two reaction mechanisms be validated reliably in these ranges; currently, they show a trend

towards a slight underestimation of the LBV for higher H_2 admixtures. The reason behind the found discrepancies and their improvement should be discussed extensively by means of the rate of production and sensitivity analysis.

3.4. Extinction Strain Rate

Having shown the comparison for the LBV, the extinction of premixed flames is also a key parameter for the validation of reaction mechanisms. Therefore, the experiments of Jackson et al. [65] were used for validation. The experimental setup was a laminar, premixed flame in counterflow flame configuration. The gases were premixed CH_4/air and CH_4/H_2/air mixtures. The authors stated that the double flame created by the opposed jet was a benchmark for assessing the effects of stretch on premixed flames for a range of fuel/air mixtures. In their setup, they investigated the lean extinction for equivalence ratios from 0.42 to 0.9.

The results and comparison to the numerical investigations performed in this work are shown in Figure 7. Both reaction mechanisms reproduce the trend of the pure CH_4 case very well (initial temperature of the gas mixture: $T_{gas} = 573$ K). There are almost no visible differences for the numerical results obtained by the two reaction mechanisms. Neither reaction mechanism can accurately reproduce the values at equivalence ratios of 0.9, and both overestimated these values. Considering the case of the H_2 admixture (90/10 CH_4/H_2, molar), it can be seen that both reaction mechanisms were again able to reproduce the trend well; however, it can be observed that the reduced mechanism shows slightly higher ESRs at equivalence ratios above 0.6 compared with the detailed reaction mechanism, which has an over-estimation of less than 5%. Still, both numerical models accurately describe the effects of the addition of H_2.

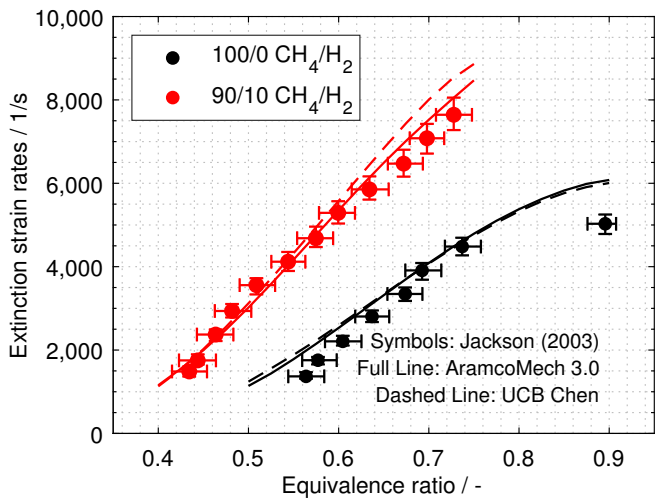

Figure 7. Experimental [65] and modeling results for the extinction strain rate of 0 and 10 mol−% H_2 in a premixed CH_4 flame ($T_{gas} = 573$ K) as a function of the equivalence ratio.

4. Conclusions

In this work, the auto-ignition of different CH_4/H_2 mixtures under stoichiometric conditions was investigated experimentally using rapid compression machine measurements. Four different fuel blends were studied in a pressure range from 6 to 15 bar and in a temperature range from 929 to 1165 K. Further, the ignition delay time, the extinction strain rate and the laminar burning velocity data in the literature were reviewed, extracted and compared to new numerical simulations for a wide range of experimental conditions with a detailed and reduced mechanism. The following observations were made:

1. In the investigated temperature range, all fuel compositions showed a linear correlation of $\log(\tau)$ to $1/T$. The apparent activation energy increased with increasing H_2 content.

2. Even small additions of H_2 to CH_4 enhanced the ignition process.
3. With further increase of the H_2 mole fraction, chain termination reactions, including C-atoms, became slightly less important.
4. In the investigated pressure/temperature range, an increase in pressure enhanced the ignition of all fuel mixtures.
5. The ignition delay times (IDT) of mixtures with a high CH_4/low H_2 mole fraction, as well as the opposite constellation, were predicted well by the reaction mechanism.
6. The laminar burning velocities (LBV) of mixtures with a high CH_4/low H_2 mole fraction were predicted well by the reaction mechanism; for a higher temperature and higher H_2 mole fraction, the mechanism showed discrepancies. A similar effect was observed by Zettervall et al. [94].
7. The extinction strain rates (ESR) for pure CH_4 and the 90/10 CH_4/H_2 were well reproduced by both reaction mechanisms.

The measurement of new IDTs over a wide temperature range showed that the reduced reaction mechanism UCB Chen [69] was able to reproduce the entire range of H_2 enrichment in CH_4. Furthermore, it was shown that satisfactory results were also obtained for the laminar burning velocity and the extinction strain rates. For some conditions, there is a lack of experimental measurements for higher hydrogen admixtures and higher temperatures, which should be the primary focus of research for future investigations. The accurate prediction of IDT, LBV and ESR encourages the use of the reaction mechanisms for simulating turbulent flames where ignition and local extinction take place.

Supplementary Materials: The following supporting information can be downloaded at: https://www.mdpi.com/article/10.3390/en16062621/s1.

Author Contributions: Conceptualization, S.D., S.E., R.S. and U.M.; Methodology, S.D., S.E. and R.S.; Software, U.M.; Validation, S.D.; Formal analysis, U.M.; Investigation, S.D., S.E. and C.Y.; Resources, R.S. and U.M.; Writing–original draft, S.D., S.E. and C.Y.; Writing–review & editing, R.S., H.K. and U.M.; Visualization, S.D. and S.E.; Supervision, R.S. and U.M.; Project administration, R.S., H. K. and U.M.; Funding acquisition, R.S., H.K. and U.M. All authors have read and agreed to the published version of the manuscript.

Funding: Financial support by the Deutsche Forschungsgemeinschaft within the framework of the DFG research group FOR 1993 "Multi-functional conversion of chemical species and energy" Project Number 229243862 and SCHI 647/3-3 is gratefully acknowledged. The authors from Freiberg gratefully acknowledge the financial support from the European Union and the state of Saxony in the ESF project (FKZ: 100284311).

Data Availability Statement: The data presented in this study are available in Supplementary Material.

Conflicts of Interest: The authors declare no conflict of interest. The funders had no role in the design of the study; in the collection, analyses, or interpretation of data; in the writing of the manuscript; or in the decision to publish the results.

Abbreviations

BB: Bunsen burner; CEV: Cardiff explosion vessel; CF: counterflow; CV: combustion vessel; EHC: external heated converging channel; ESR: extinction strain rate; HF: heat flux burner; IDT: ignition delay time; LBV: laminar burning velocity; RCM: rapid compression machine; SB: slotburner; SEF: spherical expanding flame; and ST: shock tube.

References

1. Kamil, M.; Rahman, M.M. Performance prediction of spark-ignition engine running on gasoline-hydrogen and methane-hydrogen blends. *Appl. Energy* **2015**, *158*, 556–567. [CrossRef]
2. Diéguez, P.M.; Urroz, J.C.; Sáinz, D.; Gandía, L.M. Experimental study of the performance and emission characteristics of an adapted commercial four-cylinder spark ignition engine running on hydrogen—Methane mixtures. *Appl. Energy* **2014**, *113*, 1068–1076. [CrossRef]

3. Akansu, S.O.; Bayrak, M. Experimental study on a spark ignition engine fueled by CH4/H2 (70/30) and LPG. *Int. J. Hydrogen Energy* **2011**, *36*, 9260–9266. [CrossRef]
4. Petersen, E.L.; Hall, J.M.; Smith, S.D.; de Vries, J.; Amadio, A.R.; Crofton, M.W. Ignition of Lean Methane-Based Fuel Blends at Gas Turbine Pressures. *J. Eng. Gas Turbines Power* **2007**, *129*, 937–944. [CrossRef]
5. Adolf, J.; Balzer, C.H.; Louis, J.; Fischedick, M.; Arnold, K.; Patowski, A.; Schüwer, D. *Energy of the Future? Sustainable Mobility through Fuel Cells and H_2*; Shell Deutschland Oil GmbH: Hamburg, Germany, 2017.
6. Melaina, M.W.; Antonia, O.; Penev, M. *Blending Hydrogen into Natural Gas Pipeline Networks: A Review of Key Issues*; Technical Report March; National Renewable Energy Laboratory (NREL): Golden, CO, USA, 2013. [CrossRef]
7. Yang, X.; Wang, T.; Zhang, Y.; Zhang, H.; Wu, Y.; Zhang, J. Hydrogen effect on flame extinction of hydrogen-enriched methane/air premixed flames: An assessment from the combustion safety point of view. *Energy* **2022**, *239*, 122248. [CrossRef]
8. Rudy, W.; Zbikowski, M.; Teodorczyk, A. Detonations in hydrogen-methane-air mixtures in semi confined flat channels. *Energy* **2016**, *116*, 1479–1483. [CrossRef]
9. Lowesmith, B.J.; Hankinson, G.; Johnson, D.M. Vapour cloud explosions in a long congested region involving methane/hydrogen mixtures. *Process Saf. Environ. Prot.* **2011**, *89*, 234–247. [CrossRef]
10. Bains, P.; Psarras, P.; Wilcox, J. CO_2 capture from the industry sector. *Prog. Energy Combust. Sci.* **2017**, *63*, 146–172. [CrossRef]
11. Schlögl, R. The role of chemistry in the energy challenge. *ChemSusChem* **2010**, *3*, 209–222. [CrossRef]
12. Lee, D.; Hochgreb, S. Hydrogen autoignition at pressures above the second explosion limit (0.6-4.0 MPa). *Int. J. Chem. Kinet.* **1998**, *30*, 385–406. [CrossRef]
13. Mittal, G.; Sung, C.J.; Yetter, R.A. Autoignition of H_2/CO at elevated pressures in a rapid compression machine. *Int. J. Chem. Kinet.* **2006**, *38*, 516–529. [CrossRef]
14. Gersen, S.; Anikin, N.B.; Mokhov, A.V.; Levinsky, H.B. Ignition properties of methane/hydrogen mixtures in a rapid compression machine. *Int. J. Hydrogen Energy* **2008**, *33*, 1957–1964. [CrossRef]
15. Donohoe, N.; Heufer, A.; Metcalfe, W.K.; Curran, H.J.; Davis, M.L.; Mathieu, O.; Plichta, D.; Morones, A.; Petersen, E.L.; Güthe, F. Ignition delay times, laminar flame speeds, and mechanism validation for natural gas/hydrogen blends at elevated pressures. *Combust. Flame* **2014**, *161*, 1432–1443. [CrossRef]
16. Hashemi, H.; Christensen, J.M.; Gersen, S.; Levinsky, H.; Klippenstein, S.J.; Glarborg, P. High-pressure oxidation of methane. *Combust. Flame* **2016**, *172*, 349–364. [CrossRef]
17. Kéromnès, A.; Metcalfe, W.K.; Heufer, K.A.; Donohoe, N.; Das, A.K.; Sung, C.J.; Herzler, J.; Naumann, C.; Griebel, P.; Mathieu, O.; et al. An experimental and detailed chemical kinetic modeling study of hydrogen and syngas mixture oxidation at elevated pressures. *Combust. Flame* **2013**, *160*, 995–1011. [CrossRef]
18. Bhaskaran, K.A.; Gupta, M.C.; Just, T. Shock tube study of the effect of unsymmetric dimethyl hydrazine on the ignition characteristics of hydrogen-air mixtures. *Combust. Flame* **1973**, *21*, 45–48. [CrossRef]
19. Slack, M.W. Rate coefficient for H + O_2 + M = HO_2 + M evaluated from shock tube measurements of induction times. *Combust. Flame* **1977**, *28*, 241–249. [CrossRef]
20. Wang, B.L.; Olivier, H.; Grönig, H. Ignition of shock-heated H 2 -air-steam mixtures. *Combust. Flame* **2003**, *133*, 93–106. [CrossRef]
21. Huang, J.; Hill, P.G.; Bushe, W.K.; Munshi, S.R. Shock-tube study of methane ignition under engine-relevant conditions: Experiments and modeling. *Combust. Flame* **2004**, *136*, 25–42. [CrossRef]
22. Pang, G.A.; Davidson, D.F.; Hanson, R.K. Experimental study and modeling of shock tube ignition delay times for hydrogen-oxygen-argon mixtures at low temperatures. *Proc. Combust. Inst.* **2009**, *32*, 107–118. [CrossRef]
23. Zhang, Y.; Huang, Z.; Wei, L.; Zhang, J.; Law, C.K. Experimental and modeling study on ignition delays of lean mixtures of methane, hydrogen, oxygen, and argon at elevated pressures. *Combust. Flame* **2012**, *159*, 918–931. [CrossRef]
24. Hu, E.; Pan, L.; Gao, Z.; Lu, X.; Meng, X.; Huang, Z. Shock tube study on ignition delay of hydrogen and evaluation of various kinetic models. *Int. J. Hydrogen Energy* **2016**, *41*, 13261–13280. [CrossRef]
25. Ó Conaire, M.; Curran, H.J.; Simmie, J.M.; Pitz, W.J.; Westbrook, C.K. A comprehensive modeling study of hydrogen oxidation. *Int. J. Chem. Kinet.* **2004**, *36*, 603–622. [CrossRef]
26. Petersen, E.L.; Kalitan, D.M.; Simmons, S.; Bourque, G.; Curran, H.J.; Simmie, J.M. Methane/propane oxidation at high pressures: Experimental and detailed chemical kinetic modeling. *Proc. Combust. Inst.* **2007**, *31*, 447–454. [CrossRef]
27. Lamioni, R.; Bronzoni, C.; Folli, M.; Tognotti, L.; Galletti, C. Feeding H2-admixtures to domestic condensing boilers: Numerical simulations of combustion and pollutant formation in multi-hole burners. *Appl. Energy* **2022**, *309*, 118379. [CrossRef]
28. Zhang, Y.; Wu, J.; Ishizuka, S. Hydrogen addition effect on laminar burning velocity, flame temperature and flame stability of a planar and a curved CH_4-H $_2$—Air premixed flame. *Int. J. Hydrogen Energy* **2009**, *34*, 519–527. [CrossRef]
29. Eckart, S.; Prieler, R.; Hochenauer, C.; Krause, H. Application and comparison of multiple machine learning techniques for the calculation of laminar burning velocity for hydrogen-methane mixtures. *Therm. Sci. Eng. Prog.* **2022**, *32*, 101306. [CrossRef]
30. Konnov, A.A.; Mohammad, A.; Kishore, V.R.; Kim, N.I.; Prathap, C.; Kumar, S. A comprehensive review of measurements and data analysis of laminar burning velocities for various fuel+air mixtures. *Prog. Energy Combust. Sci.* **2018**, *68*, 197–267. [CrossRef]
31. Hu, E.; Huang, Z.; He, J.; Jin, C.; Zheng, J. Experimental and numerical study on laminar burning characteristics of premixed methane–hydrogen–air flames. *Int. J. Hydrogen Energy* **2009**, *34*, 4876–4888. [CrossRef]
32. Berwal, P.; Shawnam; Kumar, S. Laminar burning velocity measurement of CH4/H2/NH3-air premixed flames at high mixture temperatures. *Fuel* **2023**, *331*, 125809. [CrossRef]

33. Braun-Unkhoff, M.; Kick, T.; Frank, P.; Aigner, M. An Investigation on Laminar Flame Speed as Part of Needed Combustion Characteristics of Biomass-Based Syngas Fuels. *Proc. ASME Turbo Expo* **2009**, *2*, 343–352. [CrossRef]
34. Boushaki, T.; Dhué, Y.; Selle, L.; Ferret, B.; Poinsot, T. Effects of hydrogen and steam addition on laminar burning velocity of methane–air premixed flame: Experimental and numerical analysis. *Int. J. Hydrogen Energy* **2012**, *37*, 9412–9422. [CrossRef]
35. Göckeler, K.; Albin, E.; Krüger, O.; Paschereit, C.O. Burning velocities of hydrogen-methane-air mixtures at highly steam-diluted conditions. In Proceedings of the fourth International Conference on Jets, Wakes and Separated Flows, ICJWSF-2013, Nagoya, Japan, 17–21 September 2013.
36. Lhuillier, C.; Oddos, R.; Zander, L.; Lückoff, F.; Göckeler, K.; Paschereit, C.O.; Djordjevic, N. Hydrogen-Enriched Methane Combustion Diluted with Exhaust Gas and Steam: Fundamental Investigation on Laminar Flames and NOx Emissions. In Proceedings of the ASME Turbo Expo 2017: Turbomachinery Technical Conference and Exposition, Charlotte, NC, USA, 26–30 June 2017; Part F1300. [CrossRef]
37. Ilbas, M.; Crayford, A.P.; Yilmaz, I.; Bowen, P.J.; Syred, N. Laminar-burning velocities of hydrogen–air and hydrogen–methane–air mixtures: An experimental study. *Int. J. Hydrogen Energy* **2006**, *31*, 1768–1779. [CrossRef]
38. Park, O.; Veloo, P.S.; Liu, N.; Egolfopoulos, F.N. Combustion characteristics of alternative gaseous fuels. *Proc. Combust. Inst.* **2011**, *33*, 887–894. [CrossRef]
39. Li, Z.; Cheng, X.; Wei, W.; Qiu, L.; Wu, H. Effects of hydrogen addition on laminar flame speeds of methane, ethane and propane: Experimental and numerical analysis. *Int. J. Hydrogen Energy* **2017**, *42*, 24055–24066. [CrossRef]
40. Cammarota, F.; Di Benedetto, A.; Di Sarli, V.; Salzano, E.; Russo, G. Combined effects of initial pressure and turbulence on explosions of hydrogen-enriched methane/air mixtures. *J. Loss Prev. Process Ind.* **2009**, *22*, 607–613. [CrossRef]
41. Halter, F.; Chauveau, C.; Djebaïli-Chaumeix, N.; Gökalp, I. Characterization of the effects of pressure and hydrogen concentration on laminar burning velocities of methane–hydrogen–air mixtures. *Proc. Combust. Inst.* **2005**, *30*, 201–208. [CrossRef]
42. Halter, F.; Chauveau, C.; Gökalp, I. Characterization of the effects of hydrogen addition in premixed methane/air flames. *Int. J. Hydrogen Energy* **2007**, *32*, 2585–2592. [CrossRef]
43. Shy, S.S.; Chen, Y.C.; Yang, C.H.; Liu, C.C.; Huang, C.M. Effects of H_2 or CO_2 addition, equivalence ratio, and turbulent straining on turbulent burning velocities for lean premixed methane combustion. *Combust. Flame* **2008**, *153*, 510–524. [CrossRef]
44. Miao, H.; Jiao, Q.; Huang, Z.; Jiang, D. Measurement of laminar burning velocities and Markstein lengths of diluted hydrogen-enriched natural gas. *Int. J. Hydrogen Energy* **2009**, *34*, 507–518. [CrossRef]
45. Tahtouh, T.; Halter, F.; Samson, E.; Mounaïm-Rousselle, C. Effects of hydrogen addition and nitrogen dilution on the laminar flame characteristics of premixed methane–air flames. *Int. J. Hydrogen Energy* **2009**, *34*, 8329–8338. [CrossRef]
46. Hu, E.; Huang, Z.; He, J.; Zheng, J.; Miao, H. Measurements of laminar burning velocities and onset of cellular instabilities of methane–hydrogen–air flames at elevated pressures and temperatures. *Int. J. Hydrogen Energy* **2009**, *34*, 5574–5584. [CrossRef]
47. Hu, E.; Huang, Z.; He, J.; Miao, H. Experimental and numerical study on lean premixed methane–hydrogen–air flames at elevated pressures and temperatures. *Int. J. Hydrogen Energy* **2009**, *34*, 6951–6960. [CrossRef]
48. Fairweather, M.; Ormsby, M.P.; Sheppard, C.G.; Woolley, R. Turbulent burning rates of methane and methane–hydrogen mixtures. *Combust. Flame* **2009**, *156*, 780–790. [CrossRef]
49. Salzano, E.; Cammarota, F.; Di Benedetto, A.; Di Sarli, V. Explosion behavior of hydrogen–methane/air mixtures. *J. Loss Prev. Process Ind.* **2012**, *25*, 443–447. [CrossRef]
50. Okafor, E.C.; Hayakawa, A.; Nagano, Y.; Kitagawa, T. Effects of hydrogen concentration on premixed laminar flames of hydrogen–methane–air. *Int. J. Hydrogen Energy* **2014**, *39*, 2409–2417. [CrossRef]
51. Troshin, K.Y.; Borisov, A.A.; Rakhmetov, A.N.; Arutyunov, V.S.; Politenkova, G.G. Burning velocity of methane-hydrogen mixtures at elevated pressures and temperatures. *Russ. J. Phys. Chem. B* **2013**, *7*, 290–301. [CrossRef]
52. Reyes, M.; Tinaut, F.V.; Horrillo, A.; Lafuente, A. Experimental characterization of burning velocities of premixed methane-air and hydrogen-air mixtures in a constant volume combustion bomb at moderate pressure and temperature. *Appl. Therm. Eng.* **2018**, *130*, 684–697. [CrossRef]
53. Khan, A.R.; Ravi, M.R.; Ray, A. Experimental and chemical kinetic studies of the effect of H2 enrichment on the laminar burning velocity and flame stability of various multicomponent natural gas blends. *Int. J. Hydrogen Energy* **2019**, *44*, 1192–1212. [CrossRef]
54. Morovatiyan, M.; Shahsavan, M.; Baghirzade, M.; Hunter Mack, J. Effect of Hydrogen and Carbon Monoxide Addition to Methane on Laminar Burning Velocity. In Proceedings of the ASME 2019 Internal Combustion Engine Division Fall Technical, Conference, ICEF 2019, Chicago, IL, USA, 20–23 October 2019. [CrossRef]
55. Cai, X.; Wang, J.; Bian, Z.; Zhao, H.; Zhang, M.; Huang, Z. Self-similar propagation and turbulent burning velocity of CH4/H2/air expanding flames: Effect of Lewis number. *Combust. Flame* **2020**, *212*, 1–12. [CrossRef]
56. Nguyen, M.T.; Luong, V.V.; Pham, Q.T.; Phung, M.T.; Do, P.N. Effect of Ignition Energy and Hydrogen Addition on Laminar Flame Speed, Ignition Delay Time, and Flame Rising Time of Lean Methane/Air Mixtures. *Energies* **2022**, *15*, 1940. [CrossRef]
57. Coppens, F.H.; De Ruyck, J.; Konnov, A.A. Effects of hydrogen enrichment on adiabatic burning velocity and NO formation in methane + air flames. *Exp. Therm. Fluid Sci.* **2007**, *31*, 437–444. [CrossRef]
58. Hermanns, R. Laminar Burning Velocities of Methane-Hydrogen-Air Mixtures. Ph.D. Thesis, Technische Universiteit Eindhoven, Eindhoven, The Netherlands, 2007. [CrossRef]
59. Dirrenberger, P.; Le Gall, H.; Bounaceur, R.; Herbinet, O.; Glaude, P.A.; Konnov, A.; Battin-Leclerc, F. Measurements of laminar flame velocity for components of natural gas. *Energy Fuels* **2011**, *25*, 3875–3884. [CrossRef]

60. Nilsson, E.J.; van Sprang, A.; Larfeldt, J.; Konnov, A.A. The comparative and combined effects of hydrogen addition on the laminar burning velocities of methane and its blends with ethane and propane. *Fuel* **2017**, *189*, 369–376. [CrossRef]
61. Jithin, E.V.; Varghese, R.J.; Velamati, R.K. Experimental and numerical investigation on the effect of hydrogen addition and N_2/CO_2 dilution on laminar burning velocity of methane/oxygen mixtures. *Int. J. Hydrogen Energy* **2020**, *45*, 16838–16850. [CrossRef]
62. Wang, Z.; Wang, S.; Whiddon, R.; Han, X.; He, Y.; Cen, K. Effect of hydrogen addition on laminar burning velocity of CH4/DME mixtures by heat flux method and kinetic modeling. *Fuel* **2018**, *232*, 729–742. [CrossRef]
63. Eckart, S.; Pizzuti, L.; Fritsche, C.; Krause, H. Experimental study and proposed power correlation for laminar burning velocity of hydrogen-diluted methane with respect to pressure and temperature variation. *Int. J. Hydrogen Energy* **2022**, *47*, 6334–6348. [CrossRef]
64. Berwal, P.; Solagar, S.; Kumar, S. Experimental investigations on laminar burning velocity variation of CH4+H2+air mixtures at elevated temperatures. *Int. J. Hydrogen Energy* **2022**, *47*, 16686–16697. [CrossRef]
65. Jackson, G.S.; Sai, R.; Plaia, J.M.; Boggs, C.M.; Kiger, K.T. Influence of H2 on the response of lean premixed CH4 flames to high strained flows. *Combust. Flame* **2003**, *132*, 503–511. [CrossRef]
66. Niemann, U.; Seshadri, K.; Forman A.. Effect of addition of a nonequidiffusional Effect of addition of a nonequidiffusional reactant to an equidiffusional diffusion flame. *Combust. Theory Model.* **2013**, *17*, 563–576. [CrossRef]
67. Eckart, S.; Rong, F.Z.; Hasse, C.; Krause, H.; Scholtissek, A. Combined experimental and numerical study on the extinction limits of non-premixed H_2/CH_4 counterflow flames with varying oxidizer composition. *Int. J. Hydrogen Energy* 2022, *in press.* [CrossRef]
68. Zhou, C.W.; Li, Y.; Burke, U.; Banyon, C.; Somers, K.P.; Ding, S.; Khan, S.; Hargis, J.W.; Sikes, T.; Mathieu, O.; et al. An experimental and chemical kinetic modeling study of 1,3-butadiene combustion: Ignition delay time and laminar flame speed measurements. *Combust. Flame* **2018**, *197*, 423–438. [CrossRef]
69. Drost, S.; Aznar, M.S.; Schießl, R.; Ebert, M.; Chen, J.Y.; Maas, U. Reduced reaction mechanism for natural gas combustion in novel power cycles. *Combust. Flame* **2021**, *223*, 486–494. [CrossRef]
70. Drost, S.; Schießl, R.; Werler, M.; Sommerer, J.; Maas, U. Ignition delay times of polyoxymethylene dimethyl ether fuels (OME2 and OME3 and air: Measurements in a rapid compression machine. *Fuel* **2019**, *258*, 116070. [CrossRef]
71. Drost, S.; Werler, M.; Schießl, R.; Maas, U. Ignition delay times of methane/diethyl ether (DEE) blends measured in a rapid compression machine (RCM). *J. Loss Prev. Process Ind.* **2021**, *71*, 104430. [CrossRef]
72. Drost, S.; Kaczmarek, D.; Eckart, S.; Herzler, J.; Schießl, R.; Fritsche, C.; Fikri, M.; Atakan, B.; Kasper, T.; Krause, H.; et al. Experimental Investigation of Ethanol Oxidation and Development of a Reduced Reaction Mechanism for a Wide Temperature Range. *Energy Fuels* **2021**, *35*, 14780–14792. [CrossRef]
73. *Pressure Measurement & Control Baratron*; Technical report; ® Manometer: Andover, MA, USA, 2008.
74. National Institute of Standards and Technology. *NIST Standard Reference Database 60*; National Institute of Standards and Technology: Gaithersburg, MD, USA, 1993. [CrossRef]
75. Kistler. *Kistler Gruppe: ThermoCOMP®-Quartz Pressure Sensor, Type 6061B*; Kistler Holding AG: Winterthur, Switzerland, 2013; pp. 1–3.
76. Burster. *Potentiometric Displacement Sensors. Models 8712, 8713*; Technical Report; Gernsbach, Germany, 2020. Available online: https://www.burster.com/fileadmin/user_upload/redaktion/Documents/Products/Data-Sheets/Section_8/8712_EN.pdf (accessed on 3 April 2022).
77. Würmel, J.; Silke, E.J.; Curran, H.J.; Ó Conaire, M.S.; Simmie, J.M. The effect of diluent gases on ignition delay times in the shock tube and in the rapid compression machine. *Combust. Flame* **2007**, *151*, 289–302. [CrossRef]
78. Maas, U.; Warnatz, J. Ignition processes in hydrogen-oxygen mixtures. *Combust. Flame* **1988**, *74*, 53–69. [CrossRef]
79. Goldsborough, S.S.; Hochgreb, S.; Vanhove, G.; Wooldridge, M.S.; Curran, H.J.; Sung, C.J. Advances in rapid compression machine studies of low-and intermediate-temperature autoignition phenomena. *Prog. Energy Combust. Sci.* **2017**, *63*, 1–78. [CrossRef]
80. Sung, C.J.; Curran, H.J. Using rapid compression machines for chemical kinetics studies. *Prog. Energy Combust. Sci.* **2014**, *44*, 1–18. [CrossRef]
81. Chen, C.J.; Back, M.H.; Back, R.A. The Thermal Decomposition of Methane. I. Kinetics of the Primary Decompositionto C_2H_6 + H_2; Rate Constant for the Homogeneous Unimolecular Dissociation of Methane and its Pressure Dependence. *Can. J. Chem.* **1975**, *53*, 3580–3590. [CrossRef]
82. Holmen, A.; Rokstad, O.A.; Solbakken, A. High-Temperature Pyrolysis of Hydrocarbons. 1. Methane to Acetylene. *Ind. Eng. Chem. Process Des. Dev.* **1976**, *15*, 439–444. [CrossRef]
83. Desgroux, P.; Gasnot, L.; Sochet, L.R. Instantaneous temperature measurement in a rapid-compression machine using laser Rayleigh scattering. *Appl. Phys. B* **1995**, *61*, 69–72. [CrossRef]
84. ANSYS Inc.; ANSYS Europe Ltd. *ANSYS Chemkin-Pro Getting Started Guide, Release 2020 R2b*; Number January; Ansys®: Canonsburg, PA, USA, 2020.
85. Eckart, S.; Cai, L.; Fritsche, C.; vom Lehn, F.; Pitsch, H.; Krause, H. Laminar burning velocities, CO and NOx emissions of premixed polyoxymethylene dimethyl ether flames. *Fuel* **2021**, *293*, 120321. [CrossRef]
86. Maas, U. Coupling of chemical reaction with flow and molecular transport. *Appl. Math.* **1995**, *40*, 249–266. [CrossRef]

87. Hirschfelder, J.O.; Curtiss, C.F.; Bird, R.B.; Mayer, M.G. *Molecular Theory of Gases and Liquids*; Wiley: New York, NY, USA, 1964; Volume 165.
88. Barlow, R.; Karpetis, A.; Frank, J.; Chen, J.Y. Scalar profiles and NO formation in laminar opposed-flow partially premixed methane/air flames. *Combust. Flame* **2001**, *127*, 2102–2118. [CrossRef]
89. Eckart, S.; Yu, C.; Maas, U.; Krause, H. Experimental and numerical investigations on extinction strain rates in non-premixed counterflow methane and propane flames in an oxygen reduced environment. *Fuel* **2021**, *298*, 120781. [CrossRef]
90. Metcalfe, W.K.; Burke, S.M.; Ahmed, S.S.; Curran, H.J. A Hierarchical and Comparative Kinetic Modeling Study of C1–C2 Hydrocarbon and Oxygenated Fuels. *Int. J. Chem. Kinet.* **2013**, *45*, 638–675. [CrossRef]
91. Van Oijen, J.A. Direct numerical simulation of autoigniting mixing layers in MILD combustion. *Proc. Combust. Inst.* **2013**, *34*, 1163–1171. [CrossRef]
92. Miyata, E.; Fukushima, N.; Naka, Y.; Shimura, M.; Tanahashi, M.; Miyauchi, T. Direct numerical simulation of micro combustion in a narrow circular channel with a detailed kinetic mechanism. *Proc. Combust. Inst.* **2015**, *35*, 3421–3427. [CrossRef]
93. Panigrahy, S.; Abd El-Sabor Mohamed, A.; Wang, P.; Bourque, G.; Curran, H.J. When hydrogen is slower than methane to ignite. *Proc. Combust. Inst.* **2022**, 1–11. *in press*. [CrossRef]
94. Zettervall, N.; Fureby, C.; Nilsson, E.J.K. Evaluation of Chemical Kinetic Mechanisms for Methane Combustion: A Review from a CFD Perspective. *Fuels* **2021**, *2*, 210–240. [CrossRef]